OsteoArthritis and Cartilage (2007) **15,** 205–211

doi:10.1016/j.joca.2006.07.008

Osteoarthritis and Cartilage

International Cartilage Repair Society

OARSI OSTEOARTHRITIS RESEARCH SOCIETY INTERNATIONAL

Quantification of ankle articular cartilage topography and thickness using a high resolution stereophotography system

S. A. Millington B.M.B.S., M.R.C.S. (Ed.)†‡*, M. Grabner Ph.D.§, R. Wozelka Mag.§, D. D. Anderson Ph.D.‖, S. R. Hurwitz M.D.¶ and J. R. Crandall Ph.D.†

† *Center for Applied Biomechanics, The University of Virginia, Charlottesville, VA, USA*

‡ *Department of Traumatology, Medical University of Vienna, Austria*

§ *Department of Computer Graphics and Vision, Technical University of Graz, Austria*

‖ *Orthopaedic Biomechanics Laboratory, University of Iowa, Iowa City, IA, USA*

¶ *Department of Orthopaedic and Trauma Surgery, Foot and Ankle Division, The University of Virginia, Charlottesville, VA, USA*

Summary

Objective: To describe the topography and to measure thicknesses, surface areas and volumes in the cartilage layers of the ankle.

Methods: Twelve cadaveric ankle joints were disarticulated and the cartilage surfaces of each bone were imaged with a highly accurate (± 2 μm) stereophotography system (ATOS™). The cartilage was then dissolved and the subchondral bone imaged. The geometric data were then used to measure the quantitative parameters in each cartilage layer.

Results: The mean cartilage volume across the 12 specimens ranged from 0.32 ± 0.08 ml for the fibula to 2.44 ± 0.48 ml for the talus. The mean thickness of both the talar (1.1 ± 0.18 mm) and tibial (1.16 ± 0.14 mm) cartilage was significantly thicker than the fibula (0.85 ± 0.13 mm). The talus had the greatest mean maximum cartilage thickness (2.38 ± 0.4 mm).

Conclusions: The reported stereophotographic technique may be used as an independent gold standard for validation of the accuracy of quantitative cartilage measurements made using magnetic resonance imaging. The thickness distribution maps show that the thickest articular cartilage occurs over the talar shoulders where osteochondral lesions commonly occur and not in the centre of the talar dome as commonly believed.

Key words: Ankle, Articular cartilage, Cartilage thickness, Cartilage volume, Stereophotography.

Introduction

Accurate quantitative descriptions of the surface geometry of articular joints are essential for validating the accuracy of measurements made using advanced 3-D magnetic resonance imaging (MRI) techniques and the development of computational models.

In order to characterise the mechanical properties of a diarthrodial joint, accurate measurements of the articular cartilage thickness and the variation in thickness across the surface of the joint are required. It is also essential to have baseline measurements of quantitative geometric parameters of cartilage, such as thickness and volume in healthy joints, if we are to use non-invasive imaging-based biomarkers to monitor the progression of degenerative joint diseases[1], such as osteoarthritis.

Most previous investigations of articular cartilage thickness have dealt with the knee. There have been relatively few studies of the ankle and other joints possessing thinner articular cartilage layers[2–5].

*Address correspondence and reprint requests to: Dr Steven A. Millington, B.M.B.S., M.R.C.S. (Ed.), Department of Traumatology, Medical University of Vienna, Leitermayergasse 31/20, A-1180 Vienna, Austria. Tel: 43-650-962-0402; Fax: 43-1-40400-7631; E-mail: steven.millington@meduniwien.ac.at

Received 6 April 2006; revision accepted 23 July 2006.

A variety of methods have been used to measure the thickness of cartilage in different joints both *in vitro* and *in vivo* with varying accuracy; *in vitro* methods include: anatomical sections[6]; needle probe measurements[7]; stereophotographic techniques[8] and A-mode ultrasound[9,10]. *In vivo* methods for measuring cartilage thickness include: X-ray measurements[11,12]; computer tomography sections[13]; and MRI[2,14]. *In vitro* techniques require disarticulation of the joint and/or may alter the thickness due to deformation during contact. Several of the *in vivo* techniques use indirect methods to make measurements of cartilage thickness e.g., X-ray and contrast-enhanced computer tomography (CT).

Early studies in this area were limited to using 2-D techniques such as anatomical sections and plain radiographs, failing to account for out-of-plane surface curvature of the joint. The resulting oblique measurements tend to over-estimate the thickness of the cartilage layer. More recent studies using advanced 3-D reconstruction techniques allowed precise thickness measurements to be made perpendicular to the joint surface, hence accommodating curvature in all directions and giving true thickness measurements at an increased number of points.

Ateshian *et al.*[8] developed an analytical stereophotographic technique for measuring the thickness of articular cartilage and applied the technique to the knee, but not to thin articular layers such as the ankle joint. The reported

technique was a non-contact method which allowed precise measurements (±90 μm). Unfortunately the process was slow, labour intensive and allowed only a discrete number of points to be digitised; furthermore, it was not possible to reconstruct the entire joint surface from one data set, as the cameras and specimen were fixed in one position.

MRI is becoming more widely available and offers many benefits over other methods for measuring articular surface geometry. Using modern segmentation algorithms and 3-D reconstruction techniques, MRI can be used to longitudinally measure changes in parameters such as cartilage thickness and volume, *in vivo*. Initial research along these lines has focused on the knee joint[14–19], which has the thickest cartilage in the body and is relatively easy to segment, as it does not have large congruent areas. However, attempts to utilise MRI for quantitative measurements of the cartilage layers of the ankle have been limited by the achievable image resolution and the techniques for detecting cartilage boundaries[20]. With the exception of the efforts of Eckstein and co-workers, there have been few attempts to establish the accuracy of MRI measurements of cartilage specifically in thin congruent cartilage layers[2–5]. Moreover, the accuracy of MRI-based quantitative measurements in thin congruent cartilage layers has not been validated against an independent gold standard.

The objectives of this study were first, to describe a high resolution stereophotographic technique for quantifying the thin cartilage layers of the ankle joint, providing a method to validate other techniques; second, to describe the topographical variation of ankle joint articular cartilage; and finally, to provide baseline measurements of quantitative parameters of ankle cartilage in joints with no visual signs of degeneration or cartilage defects.

Materials and methods

Twelve fresh frozen foot and ankle specimens were harvested from 12 male cadavers, with a mean age of 61.5 years (range 51–75 years). All specimens were acquired in accordance with state and federal laws. Ethical approval for the study was provided by the University of Virginia Institutional Review Board and human usage review panel. From the available medical histories there were no reports of trauma to the lower limbs or musculoskeletal disease in the ankle(s) of the subjects.

The specimens were stored at −25°C. Prior to testing, each specimen was allowed to thaw at room temperature for 24 h. After thawing, the ankle joints were disarticulated, and soft tissues were removed from around the tibia–fibula complex and the talus, leaving the syndesmosis intact. Each specimen was visually examined by an orthopaedic surgeon and stained using the India ink technique to assess for cartilage surface lesions and degeneration. No cartilage lesions were seen in any of the specimens tested, minor localised surface fibrillation was seen in two ankles, which is in keeping with the findings of Meachim[21] in autopsy specimens. The bones were then potted in custom potting cups using a fast-setting resin (R1 Fastcast, Goldenwest Manufacturing Inc., CA, USA) taking care to ensure that the articular surface was above the level of the potting material (Fig. 1). The talus was elevated above the potting material by inserting three screws into the inferior surface of the talus, leaving part of the screw shafts projecting into the potting material so that the screws became rigidly embedded into the resin and fixed the talus in position. During preparation the specimens were kept hydrated with phosphate buffered saline containing protease inhibitor (Sigma–Aldrich, USA). The potting cups incorporated a flange at their rim with photo targets fixed to it, the rigid fixation of the specimen ensured that there was no motion of the specimen relative to these targets (Fig. 1).

The Stereophotogrammetric system (Advanced TOpometric System – ATOS II SO, Capture 3-d, CA, USA) consists of two high resolution CCD cameras, a fringe pattern projector and digital image processing software. The ATOS system has a measurement noise (accuracy) of ±2 μm and a point spacing of 0.03 mm (http://www.gom.com/EN/measuring.systems/atos/system/variations). The system functions by projecting a fringe pattern onto the specimen and the fixed photo targets; the system then uses triangulation and digital image post processing to assign 3-D coordinates to each pixel, thereby generating a dense point cloud. By combining multiple point clouds taken from different views, a full detailed 3-D model of each surface can be generated, typically yielding on the order of 70,000 points for each cartilage or bone surface. In order to improve image contrast and optimise the performance of the ATOS system a fine coating of white powder was sprayed onto the surface being imaged.

Each cartilage surface was imaged, and the point cloud data were saved to disk. The articular cartilage was then dissolved by submerging the specimen in a 5% sodium hypochlorite solution for 6–8 h to reveal the intact subchondral bone[8]. During this process the specimen was not allowed to move relative to the photo targets due to the rigid fixation. After removal from the 5% sodium hypochlorite the specimen was again visually examined by an orthopaedic

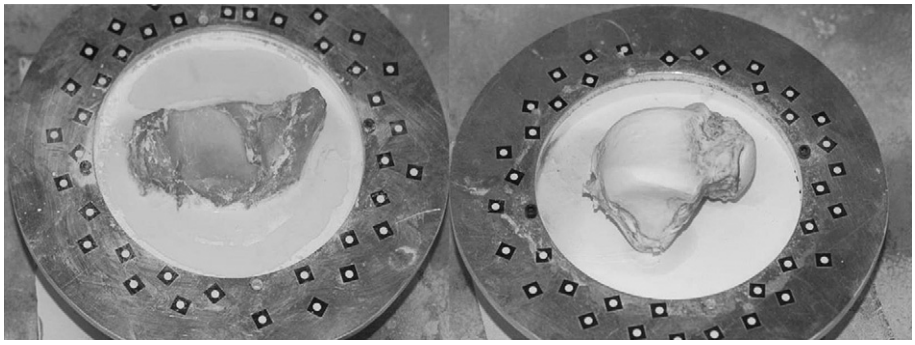

Fig. 1. A potted tibia–fibula complex and a talus specimen are shown in this picture. The articular surface of the talus has been prepared with a fine white power to improve image contrast and optimise the performance of the ATOS system. Black and white photo targets are fixed to the flange on the potting cup.

surgeon to ensure that all the cartilage had been removed. The imaging process was then repeated for the subchondral bone surfaces. Finally, the common photo targets were defined and used to spatially register the cartilage and subchondral bone surfaces together using software incorporated in the ATOS system which performs a rigid body rotation and transformation of the cartilage surface onto the bone.

POST PROCESSING TECHNIQUE

Cartilage thickness was measured by performing an octree-based search for every point on the cartilage surface to find its nearest neighbour on the corresponding bone surface. This is a reasonable approximation since the average distance between adjacent points on any surface is small, typically less than 40 μm. However, care had to be taken at the edges of the surfaces because although the cartilage and bone surfaces were registered to each other, their borders did not necessarily match identically, since the surfaces were imaged independently. If the boundary of one of the meshes were to extend beyond the other, as depicted in Fig. 2(a), an incorrectly large thickness would be reported for the extended part of the surface. These offending regions were identified by inspecting a triangle $T=(v_1,v_2,v_3)$ on M and the nearest neighbours v_i' of v_i ($i=1\ldots3$) on M', see Fig. 2(a), (v_3 is not shown in this 2-D sketch). If all v_i', $i=1\ldots3$, lie on the boundary of M', triangle T is discarded, steps 1 and 2 in Fig. 2(a). Additionally, in some specimens small amounts of periarticular tissue, e.g., fat, joint capsule and/or ligamentous tissue, which could not be completely removed caused artefacts, making the cartilage layer appear thicker along parts of the boundary [Fig. 2(b)]. Therefore, any extraneous parts at the periphery had to be identified *post hoc* and repaired. To alleviate this problem, we define a maximum thickness d_0 and shrink both meshes M and M' until the distance between them is not larger than d_0 anywhere at the boundary.

The final step was to "stitch" the cartilage and bone meshes together to form a closed volume. Note that these corrective procedures had no impact on the more central portions of the surface models, as they only occur at the periphery.

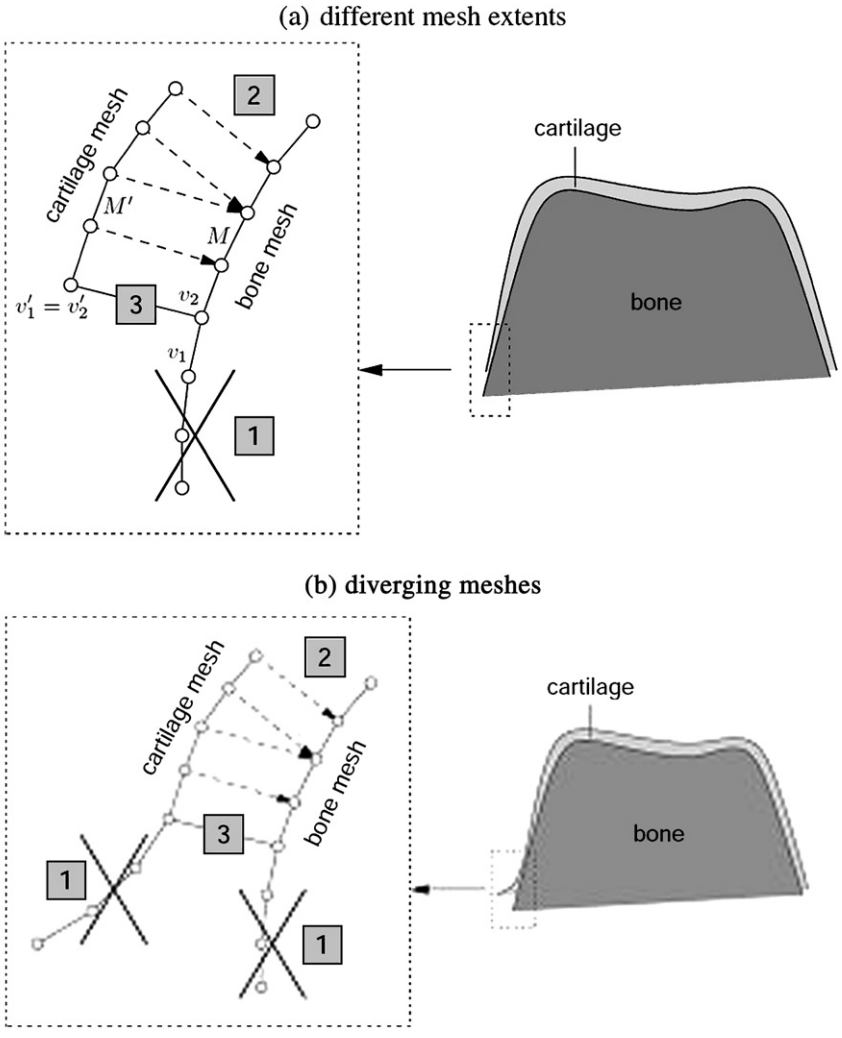

Fig. 2. Schematic of the corrective post processing procedure. (a) Different mesh extents. (b) Diverging meshes. Step 1, removal of non-corresponding regions; step 2, for each vertex on the cartilage surface the nearest neighbour on the bone surface is found; step 3, the edges of the meshes are "stitched" together.

The processed triangulated meshes for each cartilage layer were used to measure the cartilage surface areas and the bone cartilage interface (BCI) areas. The cartilage volumes were determined from the closed polyhedra formed by the combined cartilage and bone meshes. In addition, the coefficient of variation was calculated for each cartilage layer in order to provide a description of the variation of thickness within a cartilage layer.

Quantitative parameters were statistically analysed for differences between the talar, tibial and fibula layers using an ANOVA with a *post hoc* Tukey test, $P < 0.05$ was considered significant.

Results

Precise 3-D geometric models and thickness distribution maps were generated for each articular cartilage layer, providing complete geometric data including the highly curved regions and the peripheries of the surfaces. Representative examples of the 3-D thickness distribution maps are shown in Figs. 3–5. The 3-D models faithfully reproduce the sellar shape of the talus and the concavity of the distal tibial surface, and the thickness distribution maps reveal several characteristic patterns. The talus maps displayed two distinct areas over the talar shoulders, one anterior-laterally and one posterior-medially, where the thickest cartilage occurred (Fig. 3). The tibial cartilage thickness was more evenly distributed; however, the thickest cartilage typically occurred in two areas; the central part of the anterior tibial plafond and the curved region at the transition between the tibial plafond and the medial malleolus (Fig. 4). The fibula showed a characteristic valgus angulation of the distal articular surface and had the most homogeneous cartilage thickness of the ankle cartilage layers (Fig. 5).

The articular cartilage thickness was measured at every point on the articular cartilage surface; the mean number of measurements per surface was 73,236. The mean and standard deviations (across the 12 specimens) of spatial mean thickness, maximum thickness, cartilage surface area, BCI area and volume are shown in Table I.

There was no significant difference between the mean articular cartilage thickness of talar and tibial cartilage layers. The talar ($P < 0.01$) and the tibial cartilage ($P < 0.001$) spatial mean thickness values were significantly greater than the fibula cartilage. For maximum cartilage thickness the only significant difference was between the talus and the fibula ($P < 0.05$).

Cartilage surface area and BCI area measurements showed clear significant differences. The talus had a significantly larger surface area than both the tibia ($P < 0.001$) and the fibula ($P < 0.001$). Even when the tibia and fibula were combined, representing the superior half of the ankle joint, the talus had a significantly larger surface area ($P < 0.001$).

The talar cartilage volume was also significantly greater than the combined tibia–fibula cartilage volume ($P < 0.001$) and the tibia had a significantly greater volume than the fibula ($P < 0001$). This is a clear reflection of the larger area covered by articular cartilage on the talus compared with the tibia and fibula.

As an assessment of the homogeneity/inhomogeneity of the cartilage thickness across the joint surface the coefficient of variation was calculated for the superior part of the joint (the tibia–fibula complex) and the inferior part of joint (the talus). The coefficients of variation were very similar for both halves of the joint, 30.21% over the tibia–fibula complex cartilage and 30.54% over the talar cartilage.

Discussion

In this study we have described a highly accurate technique for generating 3-D geometric models and making quantitative measurements in thin cartilage layers, based on a commercially available stereophotography system, ATOS™. The system allows rapid acquisition and processing of large volumes of geometric data with a measurement noise (accuracy) of ± 2 μm. The versatility and accuracy of the technique have enabled us to study geometrical parameters of thin highly curved cartilage layers to a level of detail that has not been previously possible.

Our results show that the spatial mean cartilage thickness ranged from 0.85 ± 0.13 mm in the fibula to 1.16 ± 0.14 mm in the tibia, and maximum thickness ranged from 2.06 ± 0.08 mm in the fibula to 2.38 ± 0.4 mm in the talus. The coefficients of variation show that ankle cartilage thickness has a relatively consistent level of homogeneity throughout the joint; the values are lower than those reported in the knee joint[8], but consistent with results reported in the ankle joint[9].

A variety of techniques have been used previously to measure ankle cartilage thickness in the ankle. Using the *in vitro* needle force probe technique[7,22], mean cartilage thickness values have been reported as 1.22 mm and 1.16 mm for the talus, 1.18 mm and 1.35 mm for the tibia and 0.95 mm for the fibula. Using A-mode ultrasound in an *in vitro* study the reported mean thickness values were lower; 0.95 mm and 1.0 mm for the talus and tibia, respectively. In an MRI-based study of volunteers[2] the mean

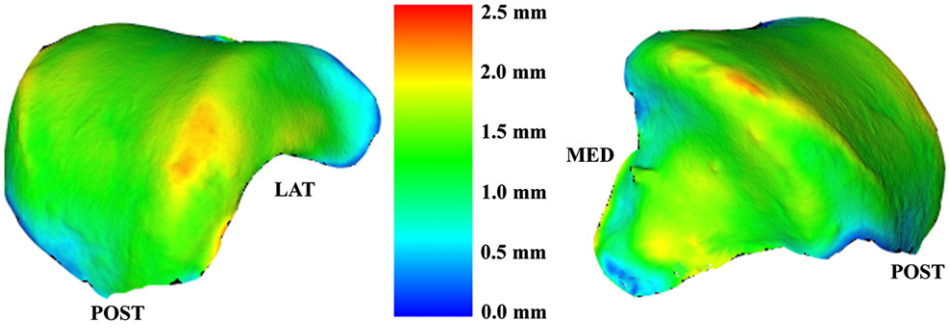

Fig. 3. Representative 3-D thickness distribution maps of the talar articular cartilage layer, viewed from the lateral (left) and medial aspects (right) of a right talus.

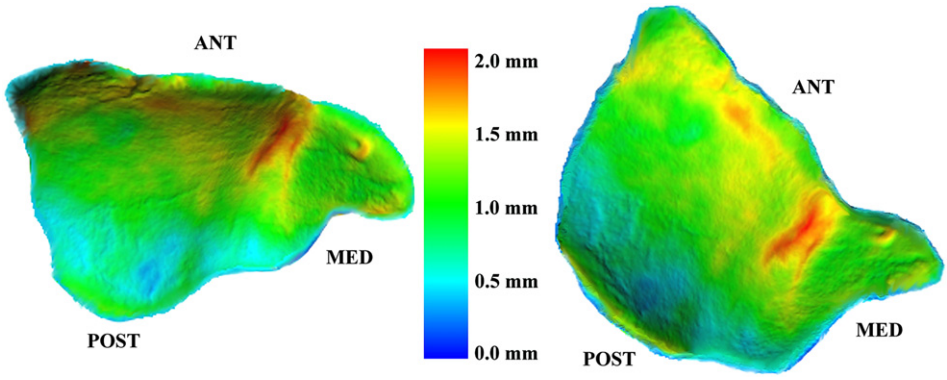

Fig. 4. Representative 3-D thickness distribution maps of the tibial articular cartilage layer, viewed from the inferior aspect of a right tibia.

cartilage thickness was at the lower limit of values reported in the literature; 0.89 mm and 0.82 mm in the talus and the tibia, respectively.

Unfortunately each of the above techniques has limitations. The needle probe technique can only be used at a number of discrete points over the surface and ruptures the surface limiting the usefulness of further testing. Furthermore, Jurvelin *et al.*[10] previously reported the change in force signal was not very sharp and a subjective evaluation was required when using a needle probe. The accuracy of ultrasound measurements is dependent on the assumption that sound travels at a uniform speed through all layers of the articular cartilage. However, previous studies[10,23] have shown considerable variation in the velocity, especially in thin cartilage layers, which may help to explain the lower mean values seen with ultrasonic measurements.

MRI can avoid many of these limitations, allowing measurements at every voxel and calculation of surface areas and volumes. Unfortunately, the earlier MRI study[2] excluded the talar shoulders and malleolar facets as well as the tibial medial malleolar and fibular surfaces, because non-isotropic sagittally acquired data were used. Therefore, a direct comparison of volume and surface area measurements with the current study is not possible.

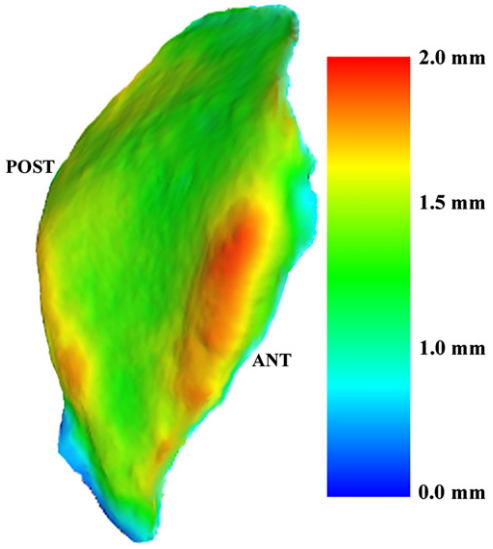

Fig. 5. A representative 3-D thickness distribution map of the fibula articular cartilage layer, viewed from the anterior aspect of a left fibula.

During the disarticulation and potting the specimens were kept hydrated with phosphate buffered saline which theoretically may result in some swelling of the articular cartilage; however, if the cartilage was left untreated it would potentially become dehydrated by exposure to the atmosphere and the surface preparation. The relatively short preparation time and the rapid data acquisition process for the cartilage surface by the ATOS™ system helped to minimise these effects; therefore, we believe that the results of the present study realistically represent the thickness of the cartilage in the *in vivo* state.

Although the reported stereophotography technique is destructive to articular cartilage, and thus can only be performed *in vitro* it is still a very useful technique as it provides an independent gold standard for validating the accuracy of other measurement techniques, such as MRI[14], which may also be used for *in vivo* studies.

In the talus the thickness distribution maps indicate the thickest cartilage region occurs anterior-laterally and posterior-medially over the shoulders of the talus. Earlier studies, unable to assess the highly curved regions of the joint surfaces, reported the thickest cartilage to occur in the central region of the talar dome[7,9,22]. Our findings are in keeping with those of Muller-Gerbl and Putz[24] who described findings from anatomical sections. The results of this study clearly show that the regions of greatest thickness on the talus correspond to the most common site of Osteochondritis dissecans (OCD) lesions in the ankle[25]. Furthermore, the thick cartilage over the anterior border of the tibia corresponds to cartilage injury sites seen in dorsiflexion testing[26]. It is also interesting to note that the regions of greatest cartilage thickness in the ankle joint correspond to regions on the talus and tibia where the subchondral bone is most dense[24]. These finding may be a response to the prevailing mechanical conditions occurring in the ankle joint.

Understanding the behaviour of ankle articular cartilage requires a true understanding of the 3-D anatomy, including

Table I
Mean values (±S.D.) for each of the quantitative parameters measured from 12 ankle specimens

$N = 12$	Talus	Tibia	Fibula
Mean thickness (mm)	1.10 ± 0.18	1.16 ± 0.14	0.85 ± 0.13
Max thickness (mm)	2.38 ± 0.4	2.18 ± 0.19	2.06 ± 0.08
Cartilage surface area (mm^2)	21.56 ± 2.14	13.45 ± 1.28	4.30 ± 0.79
BCI area (mm^2)	23.6 ± 1.67	12.57 ± 0.79	3.67 ± 0.63
Volume (ml)	2.44 ± 0.48	1.50 ± 0.28	0.32 ± 0.08

the distribution of cartilage thickness across the joint surface. Additionally, biomechanical knowledge of the cartilage stiffness distribution across the joint surface is important. As the results of this study show that the thickest cartilage occurs where cartilage injuries are most commonly seen, future studies of the cartilage mechanical properties in these regions will be of significant interest.

Changes in quantitative geometric parameters have been suggested as potentially sensitive measures of degenerative change in cartilage layers[1,27]. The described stereophotography technique offers the possibility to validate MRI derived measurement for surface areas and volumes, in addition to thickness in thin cartilage layers. Validated MRI techniques offer a powerful tool for detecting and monitoring cartilage injury and degenerative change.

The geometric data generated using this technique can be used as input to finite element (FE) computational models. As a result the geometric database created from this study may be used to generate a representative geometry of the ankle joint and its cartilage layers[28]. FE models based on representative geometry can be of significant benefit for stress and strain analyses[29] and to aid development of improved ankle prostheses[30].

Conclusions

We have reported a highly accurate technique for acquiring geometric data and making quantitative measurements of thin articular cartilage layers. The reported stereophotographic technique may be used as an independent gold standard for validation of the accuracy of *in vivo* measurements in thin cartilage layers using MRI. Furthermore, the 3-D geometric ankle cartilage data will help to produce more realistic computational models for biomechanical analysis. Finally, the thickness distribution maps produced show that the thickest articular cartilage in the ankle occurs at the clinically relevant regions where cartilage lesions most commonly occur[25].

References

1. Gray ML, Eckstein F, Peterfy C, Dahlberg L, Kim YJ, Sorensen AG, *et al*. Toward imaging biomarkers for osteoarthritis. Clin Orthop Relat Res 2004;(427 Suppl):S175–81.
2. Al Ali D, Graichen H, Faber S, Englmeier KH, Reiser M, Eckstein F. Quantitative cartilage imaging of the human hind foot: precision and inter-subject variability. J Orthop Res 2002;20(2):249–56.
3. Graichen H, Springer V, Flaman T, Stammberger T, Glaser C, Englmeier KH, *et al*. Validation of high-resolution water-excitation magnetic resonance imaging for quantitative assessment of thin cartilage layers. Osteoarthritis Cartilage 2000;8(2):106–14.
4. Peterfy CG, van Dijke CF, Lu Y, Nguyen A, Connick TJ, Kneeland JB, *et al*. Quantification of the volume of articular cartilage in the metacarpophalangeal joints of the hand: accuracy and precision of three-dimensional MR imaging. AJR Am J Roentgenol 1995;165(2): 371–5.
5. Nishii T, Sugano N, Sato Y, Tanaka H, Miki H, Yoshikawa H. Three-dimensional distribution of acetabular cartilage thickness in patients with hip dysplasia: a fully automated computational analysis of MR imaging. Osteoarthritis Cartilage 2004;12(8):650–7.
6. Jurvelin J, Kiviranta I, Arokoski J, Tammi M, Helminen HJ. Indentation study of the biochemical properties of articular cartilage in the canine knee. Eng Med 1987;16(1):15–22.
7. Shepherd DE, Seedhom BB. Thickness of human articular cartilage in joints of the lower limb. Ann Rheum Dis 1999;58(1):27–34.
8. Ateshian GA, Soslowsky LJ, Mow VC. Quantitation of articular surface topography and cartilage thickness in knee joints using stereophotogrammetry. J Biomech 1991;24(8):761–76.
9. Adam C, Eckstein F, Milz S, Putz R. The distribution of cartilage thickness within the joints of the lower limb of elderly individuals. J Anat 1998;193(Pt 2):203–14.
10. Jurvelin JS, Rasanen T, Kolmonen P, Lyyra T. Comparison of optical, needle probe and ultrasonic techniques for the measurement of articular cartilage thickness. J Biomech 1995;28(2):231–5.
11. Hall FM, Wyshak G. Thickness of articular cartilage in the normal knee. J Bone Joint Surg 1980;62(3): 408–13.
12. Karvonen RL, Negendank WG, Teitge RA, Reed AH, Miller PR, Fernandez-Madrid F. Factors affecting articular cartilage thickness in osteoarthritis and aging. J Rheumatol 1994;21(7):1310–8.
13. Eckstein F, Schnier M, Haubner M, Priebsch J, Glaser C, Englmeier KH, *et al*. Accuracy of cartilage volume and thickness measurements with magnetic resonance imaging. Clin Orthop Relat Res 1998; (352):137–48.
14. Cohen ZA, McCarthy DM, Kwak SD, Legrand P, Fogarasi F, Ciaccio EJ, *et al*. Knee cartilage topography, thickness, and contact areas from MRI: *in-vitro* calibration and *in-vivo* measurements. Osteoarthritis Cartilage 1999;7(1):95–109.
15. Faber SC, Eckstein F, Lukasz S, Muhlbauer R, Hohe J, Englmeier KH, *et al*. Gender differences in knee joint cartilage thickness, volume and articular surface areas: assessment with quantitative three-dimensional MR imaging. Skeletal Radiol 2001;30(3):144–50.
16. Raynauld JP, Kauffmann C, Beaudoin G, Berthiaume MJ, de Guise JA, Bloch DA, *et al*. Reliability of a quantification imaging system using magnetic resonance images to measure cartilage thickness and volume in human normal and osteoarthritic knees. Osteoarthritis Cartilage 2003;11(5):351–60.
17. Raynauld JP, Martel-Pelletier J, Berthiaume MJ, Labonte F, Beaudoin G, de Guise JA, *et al*. Quantitative magnetic resonance imaging evaluation of knee osteoarthritis progression over two years and correlation with clinical symptoms and radiologic changes. Arthritis Rheum 2004;50(2):476–87.
18. Eckstein F, Charles HC, Buck RJ, Kraus VB, Remmers AE, Hudelmaier M, *et al*. Accuracy and precision of quantitative assessment of cartilage morphology by magnetic resonance imaging at 3.0 T. Arthritis Rheum 2005;52(10):3132–6.
19. Eckstein F, Hudelmaier M, Wirth W, Kiefer B, Jackson R, Yu J, *et al*. Double echo steady state (DESS) magnetic resonance imaging of knee articular cartilage at 3 Tesla – a pilot study for the osteoarthritis initiative. Ann Rheum Dis 2005;26(8).
20. Tan TC, Wilcox DM, Frank L, Shih C, Trudell DJ, Sartoris DJ, *et al*. MR imaging of articular cartilage in the ankle: comparison of available imaging sequences and methods of measurement in cadavers. Skeletal Radiol 1996;25(8):749–55.

21. Meachim G. Cartilage fibrillation at the ankle joint in Liverpool necropsies. J Anat 1975;119(3):601–10.
22. Athanasiou KA, Niederauer GG, Schenck RC Jr. Biomechanical topography of human ankle cartilage. Ann Biomed Eng 1995;23(5):697–704.
23. Yao JQ, Seedhom BB. Ultrasonic measurement of the thickness of human articular cartilage *in situ*. Rheumatology (Oxford) 1999;38(12):1269–71.
24. Muller-Gerbl M, Putz R. Functional Anatomy of the Ankle Joint. The Tibial Pilon Fracture 1995, 1st edn[1], 3–25.
25. O'Farrell TA, Costello BG. Osteochondritis dissecans of the talus. The late results of surgical treatment. J Bone Joint Surg Br 1982;64(4):494–7.
26. Rudd R, Crandall J, Millington SA, Hurwitz SR, Hoglund N. Injury tolerance and response of the ankle joint in dynamic dorsiflexion. Stapp Car Crash Journal 2004;48:1–26.
27. Burgkart R, Glaser C, Hinterwimmer S, Hudelmaier M, Englmeier KH, Reiser M, *et al*. Feasibility of *T* and *Z* scores from magnetic resonance imaging data for quantification of cartilage loss in osteoarthritis. Arthritis Rheum 2003;48(10):2829–35.
28. Cohen ZA, Mow VC, Henry JH, Levine WN, Ateshian GA. Templates of the cartilage layers of the patellofemoral joint and their use in the assessment of osteoarthritic cartilage damage. Osteoarthritis Cartilage 2003;11(8):569–79.
29. Fitzpatrick DC, Otto JK, McKinley TO, Marsh JL, Brown TD. Kinematic and contact stress analysis of posterior malleolus fractures of the ankle. J Orthop Trauma 2004;18(5):271–8.
30. Cheung JT, Zhang M. A 3-dimensional finite element model of the human foot and ankle for insole design. Arch Phys Med Rehabil 2005;86(2):353–8.